Flexible and stretchable liquid metal antenna with 3D-printed, multilayered microchannels

Kento Yamagishi[1], Terry Ching[1,2,3], Nicole Chian[2], Martin Tan[2], and Michinao Hashimoto[1,2*]

[1]Digital Manufacturing and Design (DManD) Centre, Singapore University of Technology and Design, Singapore 487372, Singapore

[2]Pillar of Engineering Product Development, Singapore University of Technology and Design, Singapore 487372, Singapore

[3]Department of Biomedical Engineering, National University of Singapore, Singapore 117583, Singapore

Abstract

This paper describes a technique for fabricating multilayered liquid metal microfluidic devices by direct ink writing-based three-dimensional (3D) printing and applying them to create electronic devices requiring 3D configuration of the conductive wire. Existing 3D printing technologies have yet to simultaneously realize (1) direct printing of interconnected multilayered microchannels without supporting materials or post-processing and (2) integration of electronic components with microchannels during the process of printing. In this study, we investigated the DIW 3D printing settings to build the support-free hollow structure of the silicone sealant without the collapse of the extruded structure. Our approach allowed fabricating interconnected multilayered microchannels with through-holes between layers without any supporting material or post-processing. Many electronic devices require a 3D configuration of conductive wires (such as a jumper wire in a coil), which is difficult to realize by simple 3D printing. We took advantage of the fabricated 3D microchannels; the injection of liquid metal into a 3D multilayered microchannel with embedded electronic components allowed self-assembly of conductive wires with the components, enabling one-step fabrication of a flexible and stretchable liquid metal coil. To demonstrate a practical application, we produced (1) a skin-attachable radio-frequency identification (RFID) tag by directly printing a liquid metal antenna onto a commercial skin-adhesive plaster and (2) a freestanding flexible antenna with a light-emitting diode (LED) with a small footprint (< 12 mm $\times$ 8 mm) for potential implantable applications. Overall, our technology will offer a new capability to realize the automated fabrication of stretchable printed circuits with 3D configuration of electrical circuits consisting of liquid metals.

Introduction

This paper describes a method to fabricate elastomeric multilayered microchannels with interconnects by direct ink writing (DIW) three-dimensional (3D) printing of silicone sealant and the development of flexible and stretchable microfluidic electronics by injection of liquid metal. Existing 3D printing technologies have faced challenges in simultaneously realizing (1) direct printing of interconnected multilayered microchannels without sacrificial materials or post-processing and (2) integration of electronic components with microchannels during the process of printing. To realize them, an appropriate choice of material and a thorough regulation of printing conditions were required. This is the first report on the DIW 3D printing of self-supporting, interconnected multilayered microfluidic structures consisting of silicone elastomers. Many electronic devices require 3D interconnection of electric wire integrated with electronic components, which is not readily achieved by 3D printing. To address this challenge, we took advantage of 3D microchannels embedded with electronic components fabricated using our method. The injection of liquid metal allowed the one-step fabrication of flexible and stretchable microfluidic electronic devices with 3D conductive interconnections. As a demonstration, we fabricated a liquid metal antenna directly on a commercially available skin-adhesive plaster and demonstrated its application as a skin-attachable near-field-communication (NFC)-based radio-frequency identification (RFID) tag. In addition, a freestanding flexible antenna with an embedded light-emitting diode (LED) with a small footprint (< 12 mm $\times$ 8 mm) was also demonstrated for implantable applications. Our method has enabled rapid prototyping of 3D microfluidic platforms and will offer a new capability for the automated, digital manufacturing of multilayer stretchable printed circuits.

Microfluidic technologies have demonstrated a range of applications in chemical, biological, and electrical research fields as microfluidic mixers[1], lab-on-a-chip/point-of-care diagnosis[2, 3], organ-on-a-chip microdevices[4-6], and flexible and stretchable microfluidic electronics[7, 8]. The fabrication of microfluidic devices has been achieved by two major approaches: (1) soft lithography[9, 10] and (2) additive manufacturing[11-13]. Soft lithography has been arguably the gold standard to fabricate microchannels in elastomeric substrates (*e.g.*, polydimethylsiloxane (PDMS) and Ecoflex). Cleanroom-based microfabrication offers high resolution and accuracy, while microfluidic channels attainable via soft lithography are primarily planar. While lithography-free, rapid prototyping methods of micropatterning such as razor writing[14] have emerged, the fabrication of the 3D multilayered, interconnected microchannels would be possible only with labor-intensive processes involving PDMS molding, layer-to-layer alignment, and bonding[15]. Such manual procedures have limited the degree of automation to produce microfluidic devices.

As a promising alternative to soft lithography, additive manufacturing technologies, represented by 3D printing, have emerged as a digitally controllable, automated, and assembly-free method to fabricate microfluidic structures[16]. Stereolithography (SL)[17] and multi-jet modeling (MJM)[18, 19] have widely demonstrated the 3D fabrication of microchannels using photocurable resins. Those techniques have successfully demonstrated one-step fabrication of (1) entire multilayered microfluidic devices[20] and (2) replica molds for rapid assembly of multilayered microfluidic structures[21]. However, it is challenging to integrate functional components such as valves, pumps, and other electronic components with the microchannels during the process of printing or molding, which limits the functionality of microfluidic devices. Additionally, Young's modulus of photocurable resins used for SL and MJM (>200 MPa[22]) is higher than that of biological tissues such as skin (4-100 MPa[23]), heart (20–500 kPa[24]), and brain (0.1–16 kPa[25]). Such mechanical mismatch between printable materials and biological tissues imposes constraints on the use of SL and MJM to produce microfluidic devices that can be potentially used for wearable, implantable and tissue-interfaced applications.

Alternative to photopatterning, extrusion-based 3D printing, including fused deposition modeling (FDM) and DIW, are promising methods to achieve automated fabrication of microfluidic devices consisting of thermoplastics and curable resins. Extrusion-based 3D printing has been used to create (1) inverse structures for microchannels via sacrificial molding and (2) hollow structures for microchannels. Sacrificial structures have been successfully fabricated by both FDM and DIW[26-30], while sacrificial molding has involved fabricating molds and embedding them in a substrate, which cannot be fully automated. While direct printing of hollow structures by extrusion-based 3D printing has been demonstrated[31], direct printing of elastomeric hollow structures has been challenging because uncured inks are insufficiently robust to prevent the collapse of the extruded structures bridging the channel walls. On the contrary, if the extruded inks immediately solidify like thermoplastics used in FDM, the printed channels are difficult to modify; for example, it is challenging or impossible to integrate functional components with the microchannel during the process of printing. An appropriate elastomeric ink should be sufficiently soft to embed functional components yet sufficiently robust to maintain the bridging structure between vertical walls without collapsing for microchannels with multiple layers. This limitation has prevented the entirely printed multilayered, interconnected microfluidics with embedded functional components.

As a promising solution to solve this problem, Su *et al.* recently demonstrated DIW of self-supporting, enclosed microfluidic structures by selecting the viscoelastic ink of proper yield strength[32]. However, the covering layer (*i.e.*, the top surface of the microchannel) fabricated by this technique was not planar, but a convex structure consisting of self-supporting overhung walls within a certain angular range. Such non-planar, convex structures do not permit direct printing of the secondary, interconnected microchannels on the top. We recently demonstrated the fabrication of microfluidic devices based on DIW 3D printing of a fast-curing silicone sealant[33]. The silicone sealant was printed to form only the outlines of the intended channels and enclosed with top and bottom rigid flat plates to create channel structures. However, the rigid plates compromised the flexibility of the entire microfluidic device.

Here, we demonstrated a fully DIW-based fabrication of elastomeric multilayered microchannels consisting of the fast-curing silicone sealant. We selected a fast-curing silicone sealant as ink and regulated the printing condition so that self-supporting hollow structures could be obtained without the collapse of the extruded inks covering the channel outlines. In addition, we demonstrated a simple methodology to integrate small electronic components interfaced with the microchannel. We embedded an integrated circuit (IC) chip and light-emitting diodes (LED) in the silicone sealant, forming the outline of microchannels; these components were readily fixed in the outline of microchannels between the multiple printed layers. The injection of liquid metal into the multilayered microchannels with embedded electronic components via self-assembly, offering the fabrication of functional devices with 3D electrical circuits. The developed methods provide automated, postprocessing-free fabrication of microfluidic devices that can be applied for a wide range of applications, including tissue-interfaced wearable and implantable devices.

Experimental Design

In this work, we aimed to achieve the following objectives; (1) fabrication of microchannels with interconnected multilayered structures by DIW of elastomeric resins, (2) integration of electronic components with the microchannels during the process of printing, and (3) fabrication of flexible and stretchable microfluidic 3D circuits by injecting liquid metal into the multilayered microchannel.

DIW 3D printing is an extrusion-based layer-by-layer additive manufacturing method using a motion-controlled robot with pneumatic liquid dispensers to pattern liquid-phase inks such as prepolymers of elastomers into 3D structures from submillimeter to centimeter scales. The inks extruded out of nozzles are deposited along a digitally programmable toolpath to create 3D structures. In this study, we used a biocompatible, fast-curing silicone resin as a liquid ink to create the microchannels[33, 34]; this resin possessed a high measured viscosity at zero shear rate (~20,000 Pa s) that ensured minimum spreading rate upon extrusion and sufficient robustness to prevent a collapse of as-extruded structure within a certain length. Many other elastomeric resins based on liquid two-part prepolymers (*e.g.*, Sylgard 184, Ecoflex) are not compatible due to low viscosity (Sylgard 184: 3.5 Pa s and Ecoflex: 3–13 Pa s) that is insufficient to avoid the collapse of as-extruded structures.

As a substrate of the microfluidic antennas for skin-contact applications, we selected a commercially available polyurethane-based transparent skin-adhesive plaster, Cathereeplus^{TM} (Nichiban Co., Ltd.), due to its medically-approved biocompatibility, high moisture permeability, stretchability, thinness (~18 μm), and stable adhesion to the skin even under wet conditions. This demonstration also highlights that our method is applicable to fabricate microchannels (and associated liquid-metal-based devices) directly on the top of the commercial medial plasters.

Another unique attribute of this research was the integration of electronic components with the microchannel. Taking advantage of the softness of the uncured silicone sealant just after extruded, we embedded electronic components in the microchannel during the process of DIW 3D printing. We demonstrated that the IC chip was readily fixed in the outline of microchannels by embedding them between multiple printed layers. This technique provided stable fixation of the components under the deformation (stretching and bending) of the microfluidic structure. A conductive liquid placed into the microchannel served as stretchable wirings, providing the connection with the electrical components mounted on the microchannel. We selected a gallium-based liquid metal, galinstan, as a conductive liquid to inject into the microchannels because of its infinite stretchability, high conductivity, negligible vapor pressure, low viscosity, and low toxicity.

Results and Discussion

Overview of the study. **Figure 1** shows the conceptual illustration of this study. DIW 3D printing of silicone sealant enabled the postprocessing-free fabrication of interconnected multilayered microchannels (**Figure 1a**). During the fabrication, electronic components were readily integrated with the microchannel by fixing them between the printed layers of channel walls (**Figure 1b**). The DIW 3D printing technique offered the fabrication of microchannels on commercially available skin adhesive substrate. The injection of liquid metal into the printed microchannels provided flexible and stretchable microfluidic electronics that can be used for skin-interfaced devices. As a practical demonstration, we fabricated a skin-attachable flexible and stretchable NFC tag based on a liquid metal antenna for radio frequency identification (RFID) applications (**Figure 1c**).

Bridging test. We investigated the limitation in the distance that the printed silicone sealant was able to bridge without the collapse of the as-extruded structure. To create side walls of microchannels, we printed the silicone sealant on the glass slide in the pattern of parallel lines with different distances (0.5, 1.0, 1.5, 2.0, 2.5, 3.0, 4,0, 5.0, 6.0, 8.0, and 10.0 mm) between them. The pattern was printed with the same toolpath times to make the height of the wall ~800 μm (where the height of the single-layered printed line was ~160 μm). **Figure 2a** and **Movie S1** illustrate that that straight lines of the silicone sealant were printed at different speeds of printing (3.0, 4.5, 6.0, 7.5, and 9.0 mm s^{-1}) over the parallel lines to bridge them. The nozzle size and pneumatic pressures to extrude the ink was set constant at 27 G (tapered, inner diameter: 0.2 mm) and 300 kPa, respectively. **Figure 2b** and **Figure S1** show that the microscopic and optical images of silicone sealant were printed at different printing speeds over parallel lines with different distances, respectively. At the speed of 3.0 – 6.0 mm s^{-1} (*i.e.*, the speed of the moving nozzle), the printed silicone sealant bridged the walls with up to 4-mm distance but collapsed for a larger distance. The meandering and coiling of the extruded ink were observed at 3.0 mm/s speed for a distance of >2 mm. At the speed of 7.5 mm s^{-1}, the extruded ink successfully bridged the lines with a 10-mm distance without collapse. However, at the print speed of 9.0 mm/s, the rupture (disconnection) of the extruded ink was observed. The line width of the extruded ink decreased with the increment of printing speed (from 373 ± 53 μm at 3.0 mm s^{-1} to 245 ± 49 μm at 7.5 mm s^{-1}), but the standard deviation drastically increased at 9.0-mm s^{-1} speed (249 ± 86 μm) (**Figure 2c**). These results indicated that 9.0 mm s^{-1} of the nozzle speed was too fast for the extrusion of the silicone sealant. This bridging test indicated that the interplay between the flow rate of the ink (controlled by the pneumatic pressure to extrude the ink) and the nozzle speed determine the printability of the microchannels with straight walls. From this experiment, we found that, for our ink, nozzle size, and printing equipment, 4.5 – 7.5 mm s^{-1} of the printing speed was appropriate to bridge shorter distances than 4 mm without collapse and 7.5 mm s^{-1} was the best to bridge distange greater sthan 4 mm.

Covering and perfusion test. Next, we investigated the appropriate pitch of the toolpath to cover the channel structure with extruded ink. The pitch of the toolpath, i.e., the distance between parallelly neighboring toolpaths was digitally designed using computer-aided design (CAD) software. As the outline (*i.e.*, side-wall) of the microchannel, a strain gauge-like zig-zag structure with a channel width of 1.5 mm was printed. The toolpath for the covering layer was designed at an angle of 45 degrees to the channel direction (**Movie S2**). This covering test was performed with the constant nozzle size (27 G), pneumatic pressure (300 kPa), and printing speed (7.5 mm/s). The covering layer was printed over the channel outline with three different pitches (150, 200, and 300 μm). **Figure 2d** shows the microscopic images (top view) of the covering layer of the 150-μm pitch. To confirm that the covering layer completely covered the channel without a gap or space between the neighboring lines, we performed the perfusion test by injecting colored water into the channel. The color water was injected from one edge of the channel using a syringe with a needle (30 G) and the outlet was made by inserting another needle into the other edge of the channel. **Figure S2** illustrates filling the microchannel with the covering layer of 150-μm pitch with the color water without leakage from the channel wall or covering layer. However, for the microchannels with the covering layers of 200- and 250-μm pitch, leakage of water occurred during the injection. The results indicated that the covering layer with 150-μm pitch was appropriate to cover the channel to form closed channels.

Burst pressure test. To investigate the mechanical strength of the printed microchannel structure, the burst pressure test was performed on the 3D-printed chamber (diameter: 5 mm). **Figure 2e** and **Movie S3** show that the chamber with a single covering layer endured 40 kPa but started to expand and finally burst at 45 kPa. This bursting pressure is higher than the pressure required to flow liquid metal (galinstan) with a viscosity of 0.0024 Pa s through the microchannel with a dimension of 500 μm in diameter and 1 m in length at a flow rate of 10 μL s^{-1}, which is estimated to be ~15 kPa by the Hagen–Poiseuille equation. This result indicates that a single-layer printed cover was mechanically strong enough to hold the microchannel structure during the injection of fluid materials into the channels. The bursting pressure increased as the number of covering layers increased (**Figure 2f**). However, the flexibility of the printed microchannel was compromised due to the increase in thickness. Therefore, for fabricating multilayered channels, we used a single-layer printed cover for every layer of channels to retain the flexibility of the device.

DIW 3D printing of interconnected multilayered microchannels. We demonstrated the fabrication of vertically interconnected multilayered microchannels by DIW 3D printing. **Figure 3a** is the schematic illustration showing the configuration of each layer of single-, double-, triple- and more-layered microchannels. **Figure 3b** shows the step-by-step images of the process to fabricate a double-layered microchannel. First, a zigzag-shaped channel wall (channel width: ~750 μm, line width: ~350 μm) was printed on a substrate. In this experiment, the channel wall was fabricated by printing the same design for three layers; the height of the channel wall was ~500 μm. Second, the first channel cover was printed at an angle of 45 degrees to the channel direction. The pitch of the toolpath was 150 μm. Importantly, one end of the channel (a small chamber in the right bottom of the images of the microchannel) was not covered for the vertical interconnection between the first-layer and second-layer channels. Third, a channel wall for the second-layer channel was printed at an angle of 90 degrees to the first-layer channel. In the same way as the first-layer channel, the same design was printed for three layers. Finally, the second cover (*i.e.*, the top covering layer) was printed. When we printed multiple layers of microchannels (greater than three), the second covering layer was designed not to cover one end of the channel (opposite side to the first-layer-to-second-layer interconnection) to ensure the vertical interconnection between the second-layer and third-layer channels. Crucially, it was also demonstrated that we obtained freestanding microchannels by printing the bottom layer, with the same layer design as the top cover, on the sacrificial substrate such as water-soluble poly(vinyl alcohol) (PVA)-based film, before printing the first channel wall. This layer-by-layer procedure can be applied to realize 3D microchannels by modifying the CAD design of each layer.

Fluid injection to the multilayered microchannel. With the successful fabrication of microchannels, the injection of fluids into the DIW 3D-printed multilayered microchannels was demonstrated. **Movie S4** shows that water (colored in red with food dyes) was infused to double- and triple-layered microchannels from one end to the other by manual injection without any deformation of channels or leakage of water from the channel wall or covering layer. The punctured area on the channel wall caused by the needle (30 G; inner diameter: 0.15 mm, outer diameter: 0.3 mm) insertion was self-sealed due to the elasticity of the silicone sealant. **Figure 3c** shows the top and side views of the multilayered microchannels filled with colored water. In addition, we injected galinstan into the freestanding double-layered microchannel and demonstrated the stretchability of the liquid metal-filled microchannel (**Movie S5** and **Figure 3d**).

These demonstrations indicated that fluids were successfully infused into multilayered microchannels through the interconnects between each layer. The injection of liquid metal into the multilayered microchannel offered a stretchable 3D circuit.

Integration of NFC tags with microfluidic devices. As a demonstration of a liquid metal-based 3D circuit based on DIW-3D-printed elastomeric microchannel, we fabricated an antenna based on a liquid metal on a commercially available skin-adhesive material (CathereePlus™, thickness: 18 μm). The liquid metal antenna integrated with an NFC-based integrated circuit (IC) chip served as a flexible, stretchable, and skin-adhesive NFC tag. The substrate was prepared by spin-coating Ecoflex 0010 on the non-adhesive surface of Cathereeplus™ and heated the substrate on a hotplate to cure the Ecoflex layer (~7 μm thick). The Ecoflex layer served as a bonding layer between printed silicone sealant channel walls and polyurethane-based Cathereeplus™ substrate.

Figure 4a shows the step-by-step images of the procedure for the fabrication of NFC tags. First, we printed the silicone sealant to form the channel wall in the shape of a coil on the substrate. The coil for the antenna was designed as follows: inner radius: 11 mm, outer radius: 17.4 mm, and the number of turns: 8 to render the inductance of the coil as 2.76 μH when a conducting material was injected into the channels. The resonance frequency f_r of the antenna with the IC chip is given as following (Eq. 1);

$$f_r = \frac{1}{2\pi\sqrt{LC}} \quad (1)$$

where L and C represent the inductance of the coil and the total capacitance of the IC chip, respectively. In this study, we selected an IC chip with a capacitance of 50 pF. When we substituted 2.76 μH and 50 pF for L and C of Eq. 1, respectively, f_r was calculated as 13.5 MHz.

The IC chip was embedded in the silicone sealant, forming the channel wall after printing the first layer (channel height: ~170 µm). Then we printed four more layers of the channel wall in the same design as the first layer over the chip to fix the IC chip between the printed layers of the channel wall. We previously demonstrated that this mounting technique offered stable fixation of the components in the microchannels under different modes of deformation, such as stretching, bending, and twisting[34]. After printing the fifth layer of the channel wall, we printed the cover layer (**Movie S6**). Both ends of the coil were not covered for the vertical interconnection to the second-level channel as a jumper to connect them. Then, the secondary channel wall in the shape of a straight line was printed over the cover layer. The channel wall was printed for five layers in the same design. Finally, the cover for the secondary channel was printed.

The injection of liquid metal was performed manually using a 30 G needle (**Movie S7**). The liquid metal successfully passed through the jumper and the coil to fill the entire microchannel without leakage of liquid metal or deformation of the microchannel in the middle of injection. The punctured hole made by the needle was sealed with a small amount of uncured silicone sealant. **Figure 4b** shows the images of the microchannel filled with liquid metal. The fabricated liquid metal antenna embedded with an NFC chip showed f_r around 14 MHz, and its Q factor (q = 74.4) was higher than that of a commercial NFC tag (q = 55.4), which has the same diameter of the coil as our liquid metal antenna (**Figure 4c**). The high Q factor of the liquid metal antenna was achieved by the dimension of the liquid metal microchannel (width: ~500 µm, height: ~530 µm) that provided a lower resistance of the inductive coil than the commercial one made of thin (< 100 µm) bulk metal.

Characterizations of stretchable skin-attachable NFC tags. The skin-attached antenna needs to retain a reliable wireless powering efficiency under deformations. The antenna performance, i.e., the wireless communication efficiency, of the antenna can be attenuated under deformation. We evaluated the wireless communication property of the fabricated antenna under tension up to 100% strain for the directions along and across the jumper channel. **Figures 4d** and **4e** show the images of the antenna at 0% and 100% strain and the S11 signals of the antenna at different tensile strains (0, 20, 40, 60, 80, and 100% strains) in the direction along with the jumper, respectively. **Figures 4f** and **4g** show the images and the S11 signals of the antenna in the case where the tensile direction was across to the jumper. The resonant frequency (~14 MHz at 0% strain) shifted to low as the antenna was stretched (~12 MHz at 100% for both directions) due to the change in the inductance of the antenna. Nevertheless, the NFC-based wireless communication was possible for the antenna even at 100% strain using a standard NFC power source (1 W). Considering that the maximum induced tensile strain of the human skin is 63%[35], the fabricated liquid metal antenna exhibited sufficient stretchability to be applied as a skin-attachable device. Note that a previously reported skin-attachable liquid metal antenna showed reliable function at up to 30% uniaxial tensile strain[36]; our antenna exhibited more than three times higher stretchability (100%). We also evaluated the stability of the antenna against cyclic tensile stress at the maximum strains at 50% (**Movie S8**) and the antenna retained its initial performance (f_r = ~14 MHz, q = ~70) after 1000 cycles (**Figure S3**).

The liquid metal antenna showed conformal adhesion to the human skin even on a flexural area such as the wrist (**Figure 4h**) due to the adhesive layer of the substrate (Cathereeplus^{TM}). We demonstrated that the data (the uniform resource locator (URL) link for our laboratory website) stored in the IC chip of the skin-attached antenna was successfully read out using an NFC-enabled smartphone (**Movie S9**). The flexibility of the liquid metal antenna and the stable adhesion of the substrate to the skin was adequately demonstrated by the wrist flexion that caused the contraction of the skin (**Figure 4i**). The wireless communication efficiency was not attenuated after 200 cycles of flexion of the wrist (**Figure 4J**). Finally, we demonstrated that the NFC tag attached to the skin properly worked even after pouring water on the device for a few seconds (**Movie S10**). These results have demonstrated the flexibility, skin adhesiveness, electromechanical stability, and water resistance of the liquid metal antenna adequate to serve as a skin-attachable NFC tag.

Fabrication of flexible wireless light-emitting devices using DIW. Finally, we leveraged the capabilities of liquid metal antennas, fabricated using DIW techniques, to develop freestanding flexible wireless light-emitting devices with a small footprint (< 12 mm × 8 mm). Light-emitting devices with a small footprint offer potential medical and therapeutic applications. **Figure 5a** shows a comprehensive depiction of the step-by-step procedure employed in fabricating these devices, comprising a rectangular coil-shaped microchannel housing embedded LED chips. The fabrication started with printing silicone sealant onto a thin Ecoflex film (~ 7 µm in thickness). The silicone sealant was shaped in a rectangular coil, serving as the outline of the microchannels. Subsequently, LED chips were seamlessly incorporated into the silicone sealant, using a similar process used for embedding the IC chip. Afterward, the top of the device was closed by printing an additional layer of silicone sealants. This channel was then filled with liquid metal, which allowed the formation of a wireless light-emitting device. Notably, these embedded LEDs exhibited the capability of wireless illumination by applying an NFC charger even under deformation (*i.e.*, manual bending) (**Figure 5b)**. The resonance frequency of the fabricated liquid metal antenna was dependent on the number of embedded red LED chips (5 and 6) (**Figure 5c**).

Figure 5d shows the versatility of the liquid metal antenna, showcasing its integration with green LED chips and subsequent insertion into a plastic tube with an inner diameter of 7.2 mm. We studied the behavior of the liquid metal antenna with embedded green LED chips when subjected to bending, characterized by a radius of curvature of 3.6 mm. A discernible shift in the S11 versus frequency, from 15.0 to 16.6 MHz, was observed, with a decrease in the Q factor from 75.2 to 12.5 (**Figure 5e**). Regardless, this coil configuration did not impede the wireless activation of the embedded green LEDs via a standard NFC charger. These demonstrations exhibit the inherent potential of the fabricated wireless light-emitting devices for light-based medical applications, with a particular focus on photodynamic therapy (PDT) of cancer treatment. These devices are viable candidates as implantable light sources, catering to the specific needs of irradiating tumors situated within curved internal organs or confined to the intricate lumen of tubular organs, such as the esophagus, small intestines, and colon.

Conclusion

This study demonstrated an unprecedented method to fabricate elastomeric multilayered microchannels by DIW-based 3D printing of silicone sealant. With our method, interconnected multilayered microchannels with through-holes between layers were fabricated without any supporting material or post-processing. By optimizing the printing parameters, we achieved building the support-free hollow structure of the silicone sealant without the collapse of the extruded structure covering the channel outlines. It was demonstrated that the printed hollow structure with a single-layered lid endured 40 kPa of liquid injection pressure without leakage of the injected liquid. In addition, we demonstrated a simple methodology to integrate small electronic components interfaced with the microchannel. A small IC chip was readily fixed in the outline of microchannels between the multiple printed layers of silicone sealant. The injection of liquid metal into the coil-shaped multilayered microchannel with an embedded IC chip offered the development of a flexible and stretchable liquid metal antenna with the Q factor as high as 74.4. We fabricated the liquid metal coils directly on a commercially available skin-adhesive plaster as well as a freestanding device, both of which demonstrated electromechnical stabilities for wireless applications.

Overall, this work addressed two major challenges of creating microfluidic devices by 3D printing. We enabled direct printing of interconnected multilayered microchannels without support materials and integrated electronic components within these channels. This method can be performed on thin-film substrates, including commercial medical plasters, which enhances the applicability of the developed methods. Alternatively, the small footprint of the fabricated devices should pave the way for implantable light-emitting devices potentially suitable for therapeutic applications (*i.e.*, photodynamic therapy). The DIW 3D printing of elastomeric multilayered microchannels shall enable the automatable fabrication of 3D microfluidics, including multifunctional sensors, multi-material mixers, and 3D tissue engineering scaffolds.

Experimental Section

Materials. Glass slides (dimension: 76 mm × 52 mm × 1.2-1.5 mm, S9213, Matsunami Glass Ind., Ltd., Japan), polyurethane-based transparent skin-adhesive plaster, Cathereeplus$^{\mathrm{TM}}$ (Nichiban Co., Ltd., Japan), Ecoflex 0010 (Smooth-On Inc., USA), fast-curing silicone sealant (Wet Area Speed Seal Silicone, Selleys, Australia), silicone-based double-sided adhesive tape (No.7082, Teraoka Seisakusho Co., Ltd., Japan), LED chips (dimension: 1.6 mm × 0.8 mm × 0.25 mm, APG1608SURKC/T (red; λ_{peak} = 645 nm), APG1608ZGC (green; λ_{peak} = 515 nm), Kingbright Electronic Co., Ltd., USA), Galinstan (Changsha Rich Nonferrous Metals Co., Ltd., China) were used as purchased. IC chips (NTAG®216, NXP Semiconductors, NXP Semiconductors, Eindhoven, Netherlands) were obtained from the commercially available NFC tags (MM-NFCT2, Sanwa Supply, Japan).

Chemicals. Poly(vinyl alcohol) (PVA, M_w = ~22,000, product number: 32283-02, Kanto Chemical Co., Japan) and 1,2,3-Propanetriol (glycerol, product number: G9012, Sigma-Aldrich, USA) were used as purchased.

CAD design. The toolpath for the printing of the silicone sealant was designed in Rhinoceros® (Robert McNeel & Associates, USA). A script written in Grasshopper® (Robert McNeel and Associates, Seattle, WA) was used to convert the curve to a MuCAD code (a proprietary CAD format, Musashi Engineering Inc., Japan).

DIW of silicone sealant. The silicone sealant was printed using a commercially available liquid dispenser (SHOTmini 200 Sx and IMAGE MASTER 350 PC Smart, Musashi Engineering Inc.). The following parameters were kept constant: nozzle size = 27 G (inner diameter: 0.2 mm), nozzle velocity: 7.5 mm s^{-1}, the distance between nozzle and substrate: 100 – 200 µm.

Measurement of S11 signal. The S11 signal of the devices was measured using a transmitting circular coil made of copper wire (diameter: 15 mm; the number of turns: 3) connected to a network analyzer (miniVNA Tiny, mini Radio Solutions, USA).

Wireless powering. The wireless power was supplied to the devices by attracting a standard NFC reader-writer (ACR122U NFC Reader, Advanced Card Systems Ltd., China, output power level: 1 W).

Acknowledgements

K.Y. and M.H. thank the Digital Manufacturing and Design (DManD) Centre at Singapore University of Technology and Design (RGDM1620403), and Agency for Science, Technology and Research (A*STAR) RIE2020 AME Individual Research Grant (A1983c0039) and RIE2025 MTC Individual Research Grant (M22K2c0085) for the project funding. T.C., N.C., and M.T. thank Ministry of Education (MOE), Singapore, for the Graduate Fellowship.

Conflict of Interest

The authors declare no conflict of interest.

Data Availability Statement

The data that support the findings of this study are available from the corresponding author upon reasonable request.

Keywords

direct ink writing, 3D printing, microchannel, microfluidics

References

[1] C.-Y. Lee, W.-T. Wang, C.-C. Liu, L.-M. Fu, Passive mixers in microfluidic systems: A review, Chem. Eng. J. 288 (2016) 146-160.

[2] E. Samiei, M. Tabrizian, M. Hoorfar, A review of digital microfluidics as portable platforms for lab-on a-chip applications, Lab Chip 16(13) (2016) 2376-96.

[3] C.D. Chin, V. Linder, S.K. Sia, Commercialization of microfluidic point-of-care diagnostic devices, Lab Chip 12(12) (2012) 2118-2134.

[4] D. Huh, B.D. Matthews, A. Mammoto, M. Montoya-Zavala, H.Y. Hsin, D.E. Ingber, Reconstituting organ-level lung functions on a chip, Science 328(5986) (2010) 1662-1668.

[5] Q. Wu, J. Liu, X. Wang, L. Feng, J. Wu, X. Zhu, W. Wen, X. Gong, Organ-on-a-chip: recent breakthroughs and future prospects, BioMed. Eng. OnLine 19 (2020) 9.

[6] L.A. Low, C. Mummery, B.R. Berridge, C.P. Austin, D.A. Tagle, Organs-on-chips: into the next decade, Nature Reviews Drug Discovery 20(5) (2021) 345-361.

[7] S. Cheng, Z. Wu, Microfluidic electronics, Lab Chip 12 (2012) 2782-2791.

[8] L. Zhu, B. Wang, S. Handschuh-Wang, X. Zhou, Liquid Metal-Based Soft Microfluidics, Small 16(9) (2020) e1903841.

[9] P. Kim, K.W. Kwon, M.C. Park, S.H. Lee, S.M. Kim, K.Y. Suh, Soft Lithography for Microfluidics: a Review, Biochip Journal 2(2) (2008) 1-11.

[10] D.I. Walsh, 3rd, D.S. Kong, S.K. Murthy, P.A. Carr, Enabling Microfluidics: from Clean Rooms to Makerspaces, Trends Biotechnol. 35(5) (2017) 383-392.

[11] R. Amin, S. Knowlton, A. Hart, B. Yenilmez, F. Ghaderinezhad, S. Katebifar, M. Messina, A. Khademhosseini, S. Tasoglu, 3D printed microfluidic devices, Biofabrication 8(2) (2016) 022001.

[12] C. Meng, B. Ho, S.H. Ng, K. Ho, H. Li, Y.-j. Yoon, 3D printed microfluidics for biological applications, Lab Chip 15 (2015) 3627-3637.

[13] A. Folch, The upcoming 3D-printing revolution in microfluidics, Lab Chip 16(10) (2016) 1720-1742.

[14] S. Cosson, L.G. Aeberli, N. Brandenberg, M.P. Lutolf, Ultra-rapid prototyping of flexible, multilayered microfluidic devices via razor writing, Lab Chip 15(1) (2015) 72-76.

[15] X. Li, Z.T.F. Yu, D. Geraldo, S. Weng, N. Alve, W. Dun, A. Kini, K. Patel, R. Shu, F. Zhang, G. Li, Q. Jin, J. Fu, Desktop aligner for fabrication of multilayer microfluidic devices, Rev. Sci. Instrum. 86 (2015) 075008.

[16] A. Naderi, N. Bhattacharjee, A. Folch, Digital Manufacturing for Microfluidics, Annu. Rev. Biomed. Eng. 21 (2019) 325-364.

[17] C.I. Rogers, K. Qaderi, A.T. Woolley, G.P. Nordin, 3D printed microfluidic devices with integrated valves, Biomicrofluidics 9 (2015) 016501.

[18] R.D. Sochol, E. Sweet, C.C. Glick, S. Venkatesh, A. Avetisyan, K.F. Ekman, A. Raulinaitis, A. Tsai, A. Wienkers, K. Korner, K. Hanson, A. Long, B.J. Hightower, G. Slatton, D.C. Burnett, T.L. Massey, K. Iwai, L.P. Lee, K.S. Pister, L. Lin, 3D printed microfluidic circuitry via multijet-based additive manufacturing, Lab Chip 16(4) (2016) 668-78.

[19] A. Enders, I.G. Siller, K. Urmann, M.R. Hoffmann, J. Bahnemann, 3D Printed Microfluidic Mixers-A Comparative Study on Mixing Unit Performances, Small 15(2) (2019) e1804326.

[20] A.I. Shallan, P. Smejkal, M. Corban, R.M. Guijt, M.C. Breadmore, Cost-effective three-dimensional printing of visibly transparent microchips within minutes, Anal. Chem. 86(6) (2014) 3124-3130.

[21] C.C. Glick, M.T. Srimongkol, A.J. Schwartz, W.S. Zhuang, J.C. Lin, R.H. Warren, D.R. Tekell, P.A. Satamalee, L. Lin, Rapid assembly of multilayer microfluidic structures via 3D-printed transfer molding and bonding, Microsystems & Nanoengineering 2 (2016) 16063.

[22] S. Park, A.M. Smallwood, C.Y. Ryu, Mechanical and Thermal Properties of 3D-Printed Thermosets by Stereolithography, J. Photopolym. Sci. Technol. 32(2) (2019) 227-232.

[23] A. Kalra, A. Lowe, A.M. Al-Jumaily, Mechanical Behaviour of Skin: A Review, J. Mater. Sci. Eng. 5(4) (2016) 1000254.

[24] A. Tay, Materials meet bioelectrical and -mechanical demands of the heart, MRS Bull. 43(8) (2018) 566-567.

[25] W.J. Tyler, The mechanobiology of brain function, Nature Reviews Neuroscience 13(12) (2012) 867-878.

[26] V. Saggiomo, A.H. Velders, Simple 3D Printed Scaffold-Removal Method for the Fabrication of Intricate Microfluidic Devices, Adv. Sci. 2(9) (2015) 1500125.

[27] M.K. Gelber, R. Bhargava, Monolithic multilayer microfluidics via sacrificial molding of 3D-printed isomalt, Lab Chip 15(7) (2015) 1736-1741.

[28] D. Therriault, S.R. White, J.A. Lewis, Chaotic mixing in three-dimensional microvascular networks fabricated by direct-write assembly, Nat. Mater. 2(4) (2003) 265-271.

[29] W.H. Goh, M. Hashimoto, Dual Sacrificial Molding : Fabricating 3D Microchannels with Overhang and Helical Features, Micromachines 9 (2018) 523.

[30] W.H. Goh, M. Hashimoto, Fabrication of 3D Microfluidic Channels and In-Channel Features Using 3D Printed, Water-Soluble Sacrificial Mold, Macromolecular Materials and Engineering 303(3) (2018) 1700484.

[31] P.J. Kitson, M.H. Rosnes, V. Sans, V. Dragone, L. Cronin, Configurable 3D-Printed millifluidic and microfluidic 'lab on a chip' reactionware devices, Lab Chip 12(18) (2012) 3267-3271.

[32] R. Su, J. Wen, Q. Su, M.S. Wiederoder, S.J. Koester, J.R. Uzarski, M.C. McAlpine, 3D printed self-supporting elastomeric structures for multifunctional microfluidics, Sci. Adv. 6 (2020) eabc9846.

[33] T. Ching, Y. Li, R. Karyappa, A. Ohno, Y.-C. Toh, M. Hashimoto, Fabrication of integrated microfluidic devices by direct ink writing (DIW) 3D printing, Sens. Actuators B Chem. 297 (2019) 126609.

[34] K. Yamagishi, W. Zhou, T. Ching, S.Y. Huang, M. Hashimoto, Ultra-Deformable and Tissue-Adhesive Liquid Metal Antennas with High Wireless Powering Efficiency, Adv. Mater. 33(26) (2021) 2008062.

[35] M. Amjadi, Y.J. Yoon, I. Park, Ultra-stretchable and skin-mountable strain sensors using carbon nanotubes–Ecoflex nanocomposites, Nanotechnology 26(37) (2015) 375501.

[36] Y.R. Jeong, J. Kim, Z. Xie, Y. Xue, S.M. Won, G. Lee, S.W. Jin, S.Y. Hong, X. Feng, Y. Huang, J.A. Rogers, J.S. Ha, A skin-attachable, stretchable integrated system based on liquid GaInSn for wireless human motion monitoring with multi-site sensing capabilities, NPG Asia Mater. 9(August) (2017) e443.

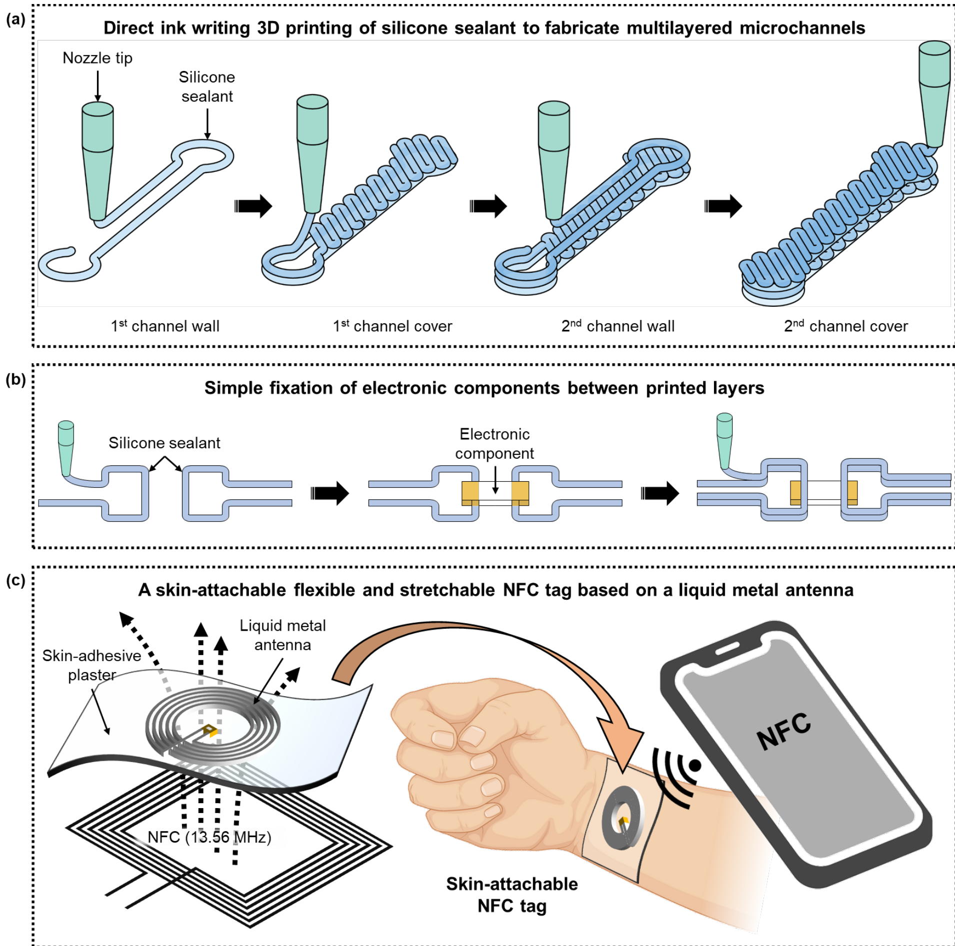

Figure 1. Overview of the research. (a) Schematic illustration of the DIW 3D printing of silicone sealant to fabricate interconnected multilayered microchannels with a through-hole between layers. (**b**) Schematic illustration of the fixation of an electronic component between printed layers of silicone sealant to integrate the component interfaced with microchannels. (**c**) Schematic illustration of a skin-attachable NFC tag based on a liquid metal antenna directly fabricated on a commercially available skin-adhesive plaster.

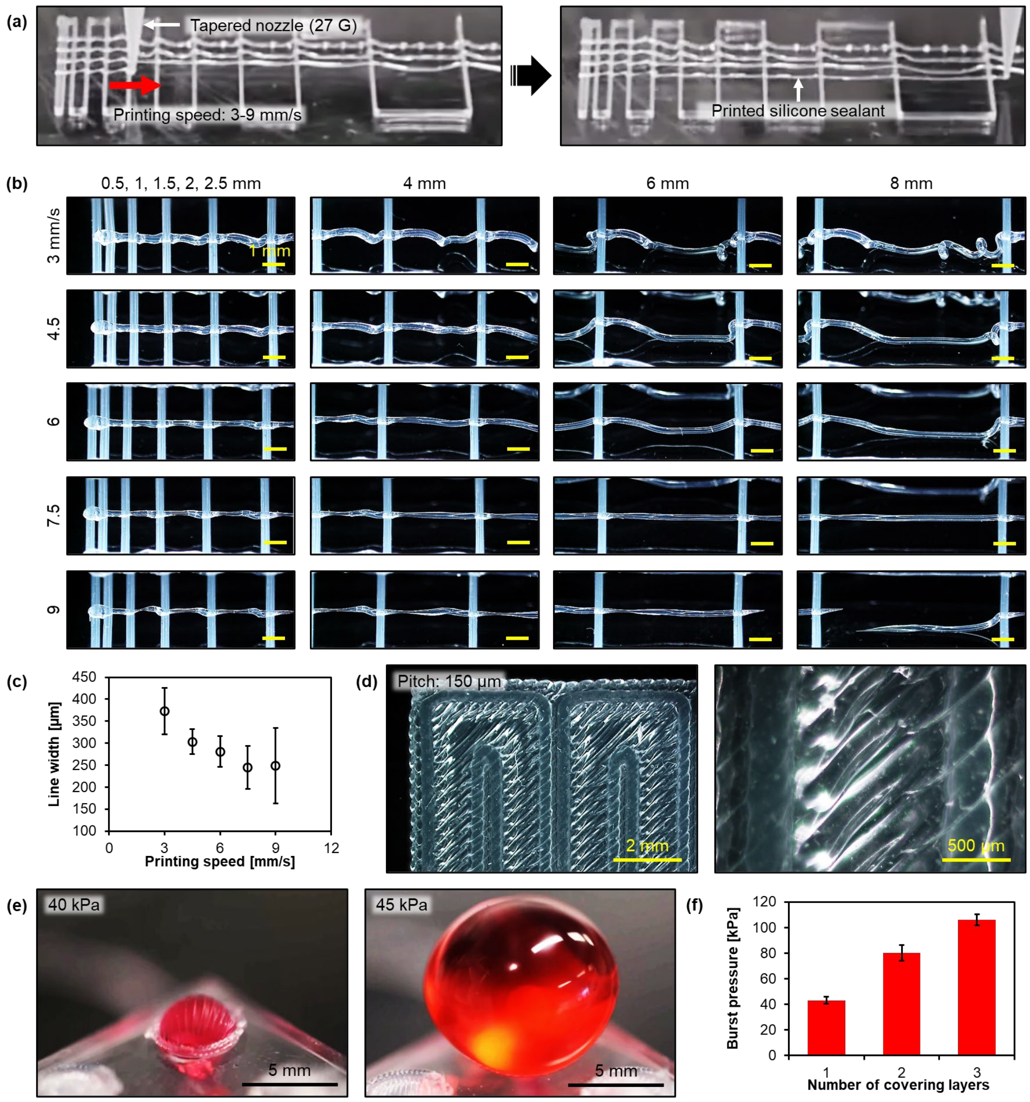

Figure 2. DIW 3D printing of silicone sealant to fabricate support-free hollow structures. (a) Images of straight lines of the silicone sealant printed over the parallel lines with different spacings. **(b)** Images of a straight line of the silicone sealant printed at different nozzle speeds over parallel lines with different spacings. **(c)** Relationship between the printing speed and the line width of the printed silicone sealant. **(d)** Images of the printed covering layer at an angle of 45 degrees to the channel direction. **(e)** Images of the printed chamber whose covering layer is expanding at the fluid pressure of 40 kPa (left) and 45 kPa (right). **(f)** Characterization of the burst pressure with respect to the number of the covering layers.

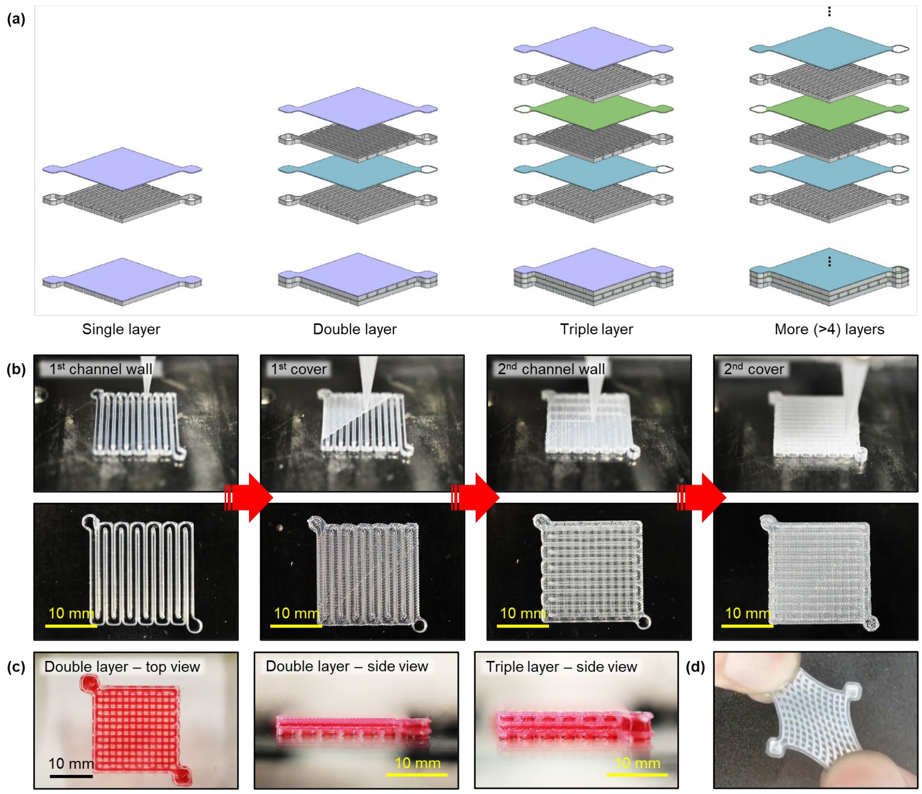

Figure 3. DIW 3D printed multilayered microchannels. (a) Schematic illustrations of single-, double-, triple-, and more (>4)-layered interconnected microchannels with through-holes. **(b)** Images of the procedure for DIW 3D printing of interconnected double-layered microchannels. **(c)** Images of interconnected double- and triple-layered microchannels filled with red-colored water. **(d)** Image of a stretched interconnected double-layered microchannel filled with liquid metal.

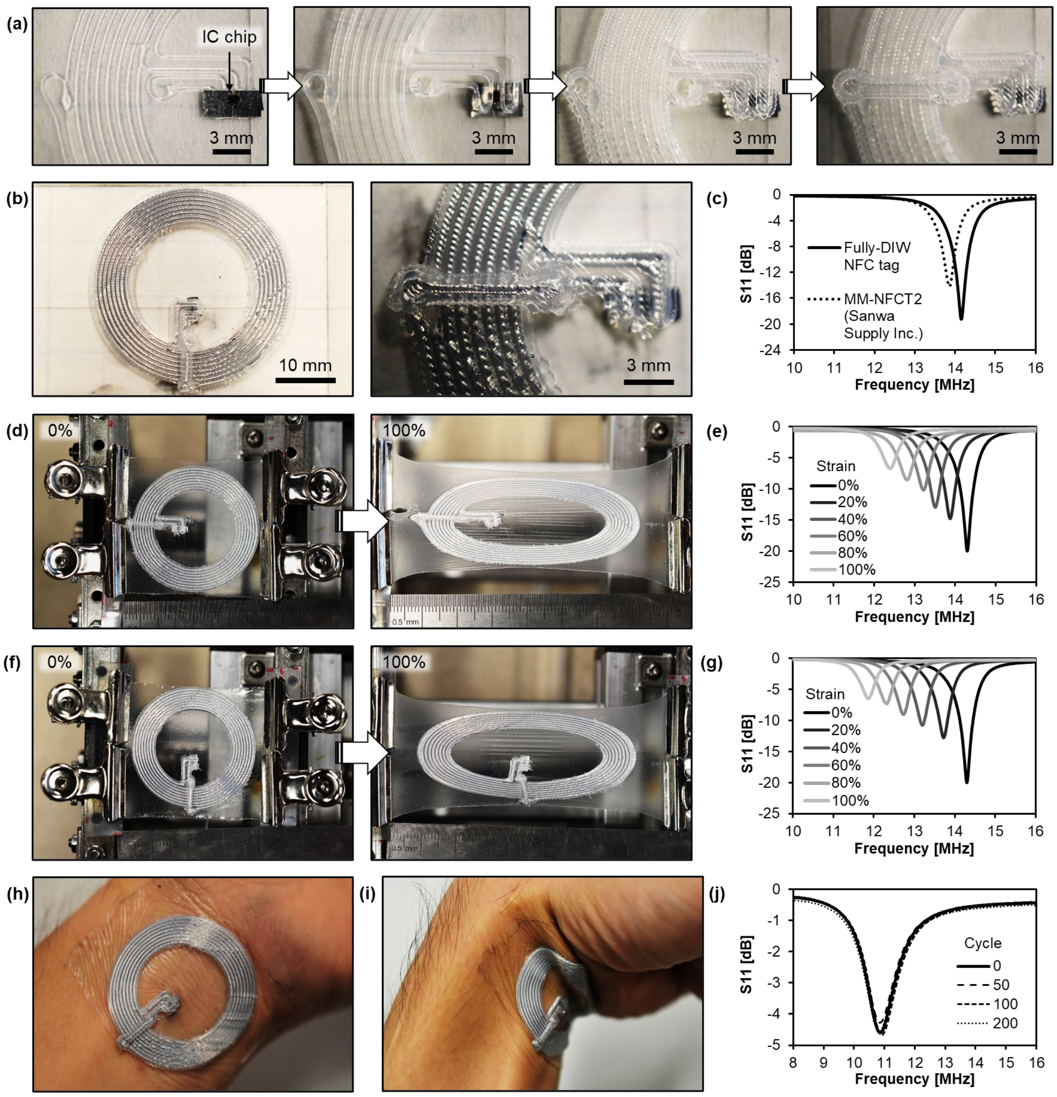

Figure 4 Skin-attachable NFC tag based on liquid metal antenna. (a) Images of the procedure for fabrication of coil-shaped microchannel with an embedded IC chip. The silicone sealant was printed on Cathereeplus^{TM} to form the channel wall in the shape of a coil on the substrate. An IC chip was embedded in the silicone sealant, forming the channel wall after printing the first layer (left). Four more layers of the channel wall were printed over the chip to fix the IC chip between the printed layers of the channel wall (second from the left). Both ends of the coil were not covered for the vertical interconnection to the second-level channel as a jumper to connect them (second from the right). The secondary channel wall in the shape of a straight line was printed over the

cover layer. The channel wall was printed for five layers in the same design. The cover layer for the secondary channel was printed (right). **(b)** Images of the microchannel filled with liquid metal. **(c)** Reflection scattering parameter (S11) versus frequency of the fabricated liquid metal antenna and a commercially available NFC tag. **(d)** Images of the liquid metal antenna at 0% (left) and 100% (right) tensile strain along the jumper channel direction. **(e)** Reflection scattering parameter (S11) versus frequency of the liquid metal antenna at different tensile strains along the jumper channel direction. **(f)** Images showing the liquid metal antenna at 0% (left) and 100% (right) tensile strain in a crosswise direction to the jumper channel. **(g)** Reflection scattering parameter (S11) versus frequency of the liquid metal antenna at different tensile strains in a crosswise direction to the jumper channel. **(h)** Image of the liquid metal antenna attached to the wrist. **(i)** Image showing the liquid metal antenna attached to the wrist in a bent state of the wrist. **(j)** Reflection scattering parameter (S11) versus frequency of the liquid metal antenna attached to the wrist after repeated cycles of bending of the wrist.

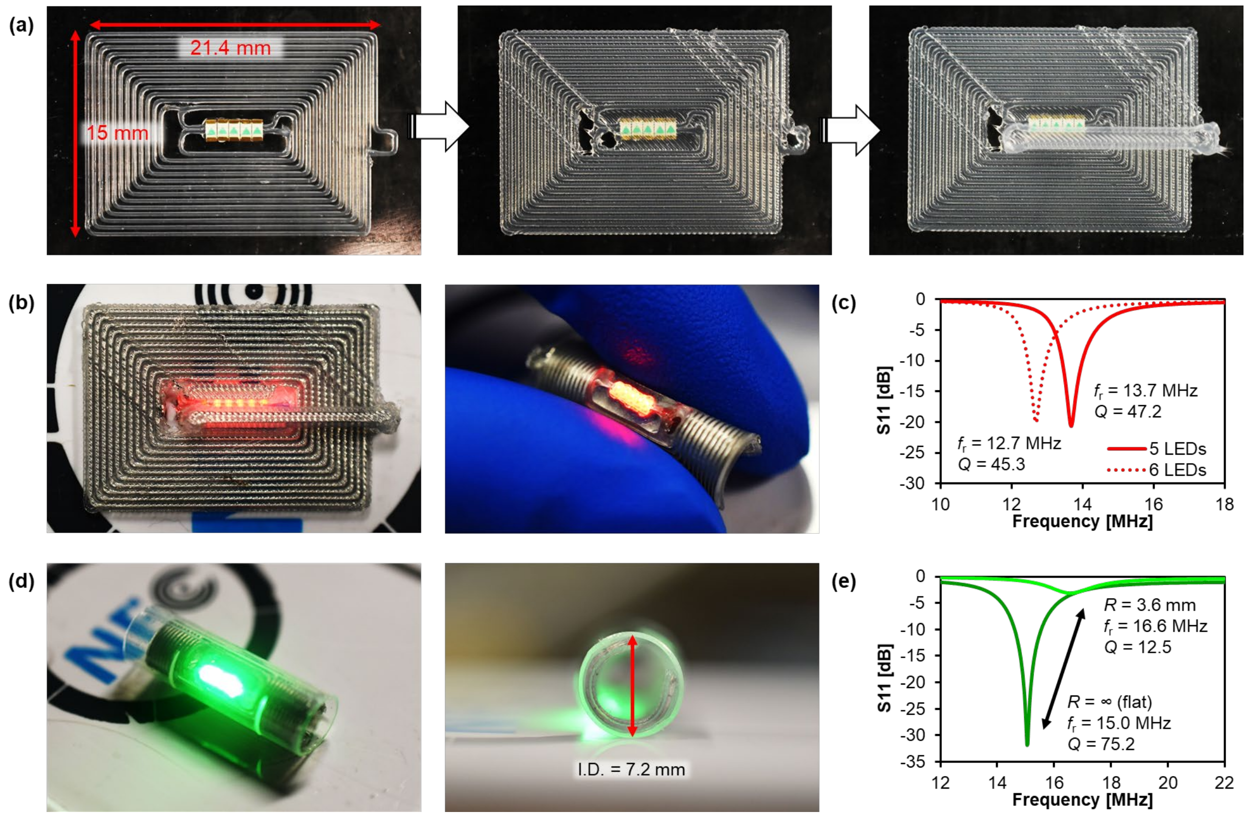

Figure 5 Flexible wireless light-emitting devices based on liquid metal coils. (a) Images of the procedure for fabricating rectangular coil-shaped microchannel with embedded LED chips. The silicone sealant was printed on Ecoflex ultrathin film with a thickness of ~7 μm to form the channel wall in the shape of a coil on the substrate. LED chips were embedded in the silicone sealant, forming the channel wall after printing the first layer (left). Four more layers of the channel wall were printed over the chip to fix the LED chips between the printed layers of the channel wall. Both ends of the coil were not covered for the vertical interconnection to the second-level channel as a jumper to connect them (middle). The secondary channel wall in the shape of a straight line was printed over the cover layer. The channel wall was printed for five layers in the same design. The cover layer for the secondary channel was printed (right). **(b)** Images of the microchannel filled with liquid metal. The embedded red LEDs were wirelessly lit up using an NFC charger (left). The fabricated flexible light-emitting device functioned even when bent by fingers (right).

(c) Reflection scattering parameter (S11) versus frequency of the fabricated liquid metal antenna with embedded different numbers of red LED chips (5 and 6). **(d)** Images of the liquid metal antenna with integrated green LED chips inserted into a plastic tube with an inner diameter of 7.2 mm. **(e)** Reflection scattering parameter (S11) versus frequency of the liquid metal antenna with embedded green LED chips in flat and bent states (radius of curvature: 3.6 mm).